



UNIVERSITÀ POLITECNICA DELLE MARCHE  
Repository ISTITUZIONALE

Osteogenic potential of dualblocks cultured with human periodontal ligament stem cells:in vitro and synchrotron microtomography study

This is a pre print version of the following article:

*Original*

Osteogenic potential of dualblocks cultured with human periodontal ligament stem cells:in vitro and synchrotron microtomography study / Manescu, Adrian; Giuliani, Alessandra; Mohammadi, S.; Tromba, G.; Mazzoni, Serena; Diomede, F.; Zini, N.; Piattelli, A.; Trubiani, O.. - In: JOURNAL OF PERIODONTAL RESEARCH. - ISSN 0022-3484. - STAMPA. - 51:1(2016), pp. 112-124. [10.1111/jre.12289]

*Availability:*

This version is available at: 11566/226809 since: 2022-05-23T16:39:00Z

*Publisher:*

*Published*

DOI:10.1111/jre.12289

*Terms of use:*

The terms and conditions for the reuse of this version of the manuscript are specified in the publishing policy. The use of copyrighted works requires the consent of the rights' holder (author or publisher). Works made available under a Creative Commons license or a Publisher's custom-made license can be used according to the terms and conditions contained therein. See editor's website for further information and terms and conditions.

This item was downloaded from IRIS Università Politecnica delle Marche (<https://iris.univpm.it>). When citing, please refer to the published version.

(Article begins on next page)

Journal of

**PERIODONTAL RESEARCH**

**Osteogenic potential of collagenated porcine Dual-blocks cultured with periodontal ligament stem cells: an in-vitro study validated by synchrotron radiation phase-contrast microtomography**

Journal:	<i>Journal of Periodontal Research</i>
Manuscript ID:	Draft
Manuscript Type:	Original Article
Date Submitted by the Author:	n/a
Complete List of Authors:	Manescu, Adrian; Università Politecnica delle Marche, Dip. di Scienze Cliniche Specialistiche e Odontostomatologiche Giuliani, Alessandra; Università Politecnica delle Marche, Dip. di Scienze Cliniche Specialistiche e Odontostomatologiche Mohammadi, Sara; Sincrotrone Trieste S.C.p.A, Tromba, Giuliana; Sincrotrone Trieste S.C.p.A, Mazzoni, Serena; Università Politecnica delle Marche, Dip. di Scienze Cliniche Specialistiche e Odontostomatologiche Diomede, Francesca; University "G. d'Annunzio", Department of Medical, Oral and Biotechnological Sciences Piattelli, Adriano; University "G. d'Annunzio", Department of Medical, Oral and Biotechnological Sciences Trubiani, Oriana; University "G. d'Annunzio", Department of Medical, Oral and Biotechnological Sciences
Keywords:	Tissue Engineering, Stem Cells, Periodontal ligament, Biomaterial

SCHOLARONE™  
Manuscripts

Osteogenic potential of collagenated porcine Dual-blocks cultured with periodontal  
ligament stem cells: an in-vitro study validated by synchrotron radiation phase-contrast  
microtomography

Osteogenic potential of hPDLSC cultured scaffolds

A. Manescu<sup>1</sup>, A. Giuliani<sup>1\*</sup>, S. Mohammadi<sup>2</sup>, G. Tromba<sup>2</sup>, S. Mazzoni<sup>1</sup>, F. Diomedè<sup>3</sup>,  
A. Piattelli<sup>3</sup>, O. Trubiani<sup>3</sup>

<sup>1</sup>Università Politecnica delle Marche, Dipartimento di Scienze Cliniche Specialistiche e  
Odontostomatologiche – Sezione di Biochimica, Biologia e Fisica, Via Brece Bianche  
1, 60131 Ancona, Italy

<sup>2</sup>Sincrotrone Trieste S.C.p.A, Strada Statale 14 - km 163.5 in AREA Science Park,  
34149 Basovizza (Trieste), Italy

<sup>3</sup> University of Chieti-Pescara, Department of Medical, Oral and Biotechnological  
Sciences, Laboratory of Stem Cells and Regenerative Medicine, Via dei Vestini 31,  
66100 Chieti, Italy

\* Corresponding author: Alessandra Giuliani, Università Politecnica delle Marche,  
Dipartimento di Scienze Cliniche Specialistiche e Odontostomatologiche – Sezione di  
Biochimica, Biologia e Fisica, Via Brece Bianche 1, 60131 Ancona, Italy, Tel. +39  
071 2204603, Fax. +39 071 2204605, Email: a.giuliani@univpm.it

## Abstract

Objective: In the present study, the early stages of *in vitro* bone formation in collagenated porcine scaffolds cultured with Periodontal Ligament Cells (hPDLSCs) were investigated. The comparison between the osteogenic potential of this structure in basal and differentiating culture media was explored to predict the mechanism of its biological behavior as graft in human defect. Results were validated by Synchrotron Radiation X-ray phase contrast micro computed tomography (SR micro-CT).

Background: The restoration of large bony maxillofacial defects represents one of the tissue engineering main challenges. It has been recently explored using cells and tissues developed *in vitro* that should ideally be immunologically, functionally, structurally and mechanically identical to the native tissue.

Method: *In vitro* cultures of human PDLSCs, easily obtained by scraping of alveolar crestal and horizontal fibers of the periodontal ligament, were seeded onto collagenated porcine blocks constituted by natural cancellous and cortical bone. 3D images were obtained by SR micro-CT and processed with the phase-retrieval algorithm based on the Transport of Intensity Equation (TIE).

Results: This work proved the *in-vitro* osteogenic potential of collagenated Dual-Blocks cultured with hPDLSCs (regardless of the culture medium) and demonstrate the capability of phase-contrast micro-CT analysis to study newly bone formation on collagenated bioscaffolds.

Conclusion: The chosen method successfully and quantitatively monitored the early stages of bone formation and the rate of the bioscaffold resorption in basal and differentiating culture media.

1  
2  
3  
4  
5  
6  
7  
8  
9  
10  
11  
12  
13  
14  
15  
16  
17  
18  
19  
20  
21  
22  
23  
24  
25  
26  
27  
28  
29  
30  
31  
32  
33  
34  
35  
36  
37  
38  
39  
40  
41  
42  
43  
44  
45  
46  
47  
48  
49  
50  
51  
52  
53  
54  
55  
56  
57  
58  
59  
60

**Keywords:** Human periodontal ligament stem cells; bone regeneration; phase contrast tomography; synchrotron radiation.

Manuscript proof

## 1. Introduction

Large bony maxillofacial defects are currently repaired by free tissue transfer with microvascular reanastomosis of vascularized flaps from distant sites including fibula, iliac crest, scapula, and radius (1, 2). These procedures have proven to be reliable and effective but require extended hospitalization and a secondary donor site where associated morbidity and complications could occur (3). Bone tissue engineering combined to gene therapy and stem cell biology is considered a promising alternative to the autologous approach. Manipulating cells, biomaterial scaffolds and cell signaling factors to regenerate large skeletal defects offers several potential benefits, including the lack of donor site, morbidity, decrease in technical sensitivity of the repair, and most importantly, the ability to closely mimic the *in vivo* microenvironment.

The restoration of damaged functions represents the main goal of contemporary medical research, using cells and tissues developed *in vitro* that should ideally be immunologically, functionally, structurally and mechanically identical to the native tissue.

However, the affirmation stating that the optimal bone construct for repair would exactly replicate the lost structure is very controversial. Indeed, if this statement is well accepted in standard tissue conditions, clinical cases presenting defects with compromised tissue beds, like in the elderly or in patients with bone reabsorption caused by disease, suggest innovative approaches (4).

Recent reports have shown that many adult tissues contain a population of stem cells (SCs) identified in the stromal tissue like bone marrow, spleen, and thymus. These are postnatal stem cells able to self-renew and regenerate lineages as bone, cartilage, tendon, skeleton muscle, neuron and oral tissue<sup>5</sup>.

In particular, a stem cells population found in the human periodontal ligament (hPDL), expressing a variety of stemness markers as CD29, CD90,CD44, CD 73, CD105, CD166, nanog, SSEA-4, oct-4, has been described (6,7).

The human Periodontal Ligament Stem Cells (hPDLSCs), easily obtainable by scraping of alveolar crestal and horizontal fibers of the periodontal ligament, are receiving extensive attention for the immense potential for tissue regeneration, since exhibit high proliferative capacity, immunomodulatory property, potential to differentiate into osteogenic, adipogenic, and chondrogenic lineages, and moreover, they possess the capacity to generate new bone following ectopic transplantation (8-10).

However, a major factor hampering such endeavors is that the environment where stem cells grow or are seeded has critical but poorly understood effects on their fate (11-16). Choosing chemical composition and internal structure of a scaffold are major decisions involving a variety of parameters such as phase composition, porosity, pore size and interconnectivity. These factors affect the transportation of nutrients that enable cell growth and proliferation and make the scaffold a suitable template for tissue growth and, eventually, osteodifferentiation, bone tissue formation, and vascularization (9, 17-19).

In this context, it has to be stressed that the kinetics of early stage *in vitro* bone formation is still unclear. Routine laboratory protocols typically subject tissue-engineered specimens only to histological analysis and electron microscopy examination, to characterize their constituent elements in 2D (9, 20). 3D visualization techniques have been demonstrated to achieve a greater understanding. X-ray computed microtomography (micro-CT), one of the most common 3D imaging techniques, has been applied to the qualitative and quantitative evaluation of tissue growth under

different conditions, including engineered bone (4, 14, 16-19, 21) and tendon (22). However, data regarding the application of X-ray-based techniques to complex constructs such those referred to early stages of *in vitro* culture of collagenated scaffolds cultured with stem cells are still limited. Whereas soft tissue investigation by attenuation-based X-ray imaging methods without contrast agents is hampered by poor contrast, phase-sensitive techniques afford enhanced contrast where absorption is insufficient, for instance to detect cells, extracellular matrix (ECM) and vessel structures. Phase-contrast X-ray imaging (PCI) is sensitive to light elements such as hydrogen, carbon, nitrogen and oxygen, which are commonly found in soft tissue. The phase contrast arises because both the amplitude and phase are modified as the X-ray beam propagates through tissue. Since the probability for X-ray phase shift can be 1000 times greater than for X-ray attenuation in the keV energy range, PCI affords visualization of soft tissues with identical or similar attenuation characteristics, which would not be detected using conventional attenuation-based imaging methods. Moreover, because the refractive index-based image contrast decreases less rapidly with increasing X-ray energy compared with attenuation-based contrast, PCI enables reduction of the delivered radiation dose (23).

Unfortunately the simpler PCI settings do not automatically provide quantitative phase data, meaning that phase-retrieval algorithms (24-26) are often required.

In this work we showed the *in-vitro* osteogenic potential of collagenated Dual-Blocks cultured with hPDLSCs, regardless of the culture medium. We also demonstrated that PCI micro-CT combined with a single distance phase-retrieval algorithm is a suitable method to study *in vitro* the early stages of bone formation. In this direction the present



research offers a new approach with a clinical advantage in the evaluation of regenerative cranio-facial surgery.

**2. Materials and methods**

**2.1. Scaffold material**

The scaffold material is named OsteoBiol® Dual-Block (Tecnoss® Dental, Coazze (TO), Italy). It is a collagenated porcine block constituted by natural cancellous and cortical bone. The peculiarity is represented by the cortical bone which is naturally anchored to cancellous bone in order to provide stability after grafting. This scaffold guarantees, due to its rigid consistency, that the original volume of grafting site can be preserved. It is indicated for horizontal crest reconstructions.

**2.2. Isolation and culture of human Periodontal Ligament Stem Cells (hPDLSCs).**

The hPDLSCs were obtained from fragments of periodontal ligament tissue from third molar teeth, scheduled to be removed for orthodontic purposes. Teeth were selected from healthy patients ranging from 20 to 35 years old. Before extraction, each subject underwent complete medical anamnesis for systemic and oral infections or diseases. All patients provided written consent for clinical research and for the processing of personal data. All teeth samples were de-identified. The periodontal ligament tissue was collected after tooth extraction. Explants were obtained from alveolar crestal and horizontal fibers of the periodontal ligament by scraping the roots of non-carious third molar teeth with a Gracey's curette (27).

The hPDLSCs were cultured in MSCM medium (Lonza Verviers Company, Basel, Belgium) according to *Trubiani et al* (10). Briefly, the adherent cells migrating from the explants were isolated using 0.1% trypsin solution and plated in tissue culture

polystyrene flasks at  $1 \times 10^3$  cells/cm<sup>2</sup>. Primary cultures of PDLSCs mainly consisted of colonies of bipolar fibroblastoid cells which, after subcultivation, proliferate with a population-doubling time of 48 h reaching a confluent growth-arrested condition.

Confluent hPDLSCs were divided in 4 different type of cultures: hPDLSCs cultured without Dual-Block in MSCM medium (ctrl@group); hPDLSCs cultured without Dual-Block in MSCM medium supplemented with hMSC Osteogenic single quotes (Lonza) (Diff@group); hPDLSCs cultured with Dual-Block in MSCM medium (DB-ctrl@group); hPDLSCs cultured with Dual-Block in MSCM medium supplemented with hMSC Osteogenic single quotes (DB-Diff@group).

The cells were seeded at  $3 \times 10^3$  cells/cm<sup>2</sup>, the medium was changed every 3 days and at each medium change the culture was examined to be sure that the monolayer was intact.

After 3 weeks of incubation the progressive mineralization was evaluated.

All experiments were carried out using cells at the 2<sup>nd</sup> passage and repeated with 3 different cell samples from 3 different patients.

### 2.3. Cytofluorimetric assay

Antibodies. Fluorescein isothiocyanate-conjugated anti-CD13 (CD13 FITC), phycoerythrin-conjugated anti-CD29 (CD29 PE), FITC-conjugated: anti-CD44 (CD44 FITC), anti-CD45 (CD45 FITC), anti-CD105 (CD105 FITC) and anti-CD166 (CD166 FITC) were obtained from Ancell (MN, USA); FITC-conjugated anti-CD14 (CD14 FITC) and PE-conjugated anti-CD133 (CD133 PE) were purchased from Milteny Biotec (Bergisch Gladbach, Germany); PE-conjugated anti-CD73 (CD73 PE), FITC-conjugated anti-CD90 (CD90 FITC), allophycocyanin-conjugated anti-CD117 (CD117-APC), PE-conjugated anti-CD146 (CD146 PE), PE-conjugated anti-CD271 (CD271-PE), Alexa488-conjugated anti-Sox2 (Sox2 Alexa488), FITC-conjugated anti-SSEA4

(SSEA4 FITC), Alexa488-conjugated anti-HLA ABC (HLA-ABC Alexa488), PE-conjugated anti-HLA-DR (HLA-DR PE) and PE-conjugated anti-OCT3/4 (OCT3/4 PE) obtained from Becton Dickinson (BD, San Jose, CA); FITC-conjugated anti-CD144 (CD144-FITC) was obtained from Acris Antibodies (Herford, Germany); PE-conjugated anti-CD34 (CD34-PE) was purchased from Beckman Coulter (Fullerton, CA, USA); appropriate secondary FITC-conjugated antibody was obtained from Jackson ImmunoResearch Laboratories (West Grove, PA, USA).

**2.4. Cell Staining for Flow Cytometry**

Washing buffer (phosphate buffered saline, PBS, 0.1 % sodium azide and 0.5 % bovine serum albumine, BSA) was used for all washing steps (3 ml of washing buffer and centrifugation, 400 xg 8 min at 4°C). Briefly, 5 x 10<sup>5</sup> cells/sample were incubated with 100 µl of 20 mM ethylenediaminetetraacetic acid (EDTA) at 37°C for 10 min and washed.

Staining of surface antigens and intracellular antigens was carried out according to *Eleuterio et al.*(6)

**2.5. Flow Cytometry Measurement**

Quality control included regular check-up with Rainbow Calibration Particles (BD Biosciences). Debris was excluded from the analysis by gating on morphological parameters; 20,000 non-debris events in the morphological gate were recorded for each sample. To assess non-specific fluorescence we used specific irrelevant controls. All antibodies were titrated under assay conditions and optimal photomultiplier (PMT) gains were established for each channel. Data were analysed using FlowJo™ software

(TreeStar, Ashland, OR). Mean Fluorescence Intensity Ratio (MFI Ratio) was calculated dividing the MFI of positive events by the MFI of negative events.

## 2.6. MTT assay and Trypan blue exclusion test

The viability of hPDLSCs, in control cultures (ctrl) and seeded onto Dual-Block scaffolds (DB-ctrl), was measured by the quantitative colorimetric MTT (3-[4,5-dimethyl-2-thiazolyl]-2,5-diphenyl-2H-tetrazoliumbromide test) (CellTiter 96®, Promega, Milan, Italy).  $2 \times 10^2$  cells/well were seeded into a 96-well culture plate with MSCM medium. After 24 h of incubation at 37°C, 15 µl/well of MTT was added to culture medium, and cells were incubated for 3 hrs at 37°C. The supernatants were read at 650 nm wavelength using a microplate reader (Sinergy HT, Biotek Instruments, Winooski, VT, USA). The MTT assay was performed in three independent experiments, six replicate wells for 24, 48, 72h and 1 week. Additionally, cell viability and proliferation were evaluated at 24, 48, 72 h and 1 week by trypan blue staining. Cells were analysed by an inverted light microscope (Leica DMIL; Leica Microsystems S.p.A., Milan, Italy). Dead cells would take up dyes and were stained blue, and surviving cells would be refractive without taking up dyes.

## 2.7. Preparation for scanning electron microscopy

The samples were fixed for 1 h at 4 °C in 2.5 % glutaraldehyde in 0.1M cacodylate buffer (pH 7.4), dehydrated in increasing ethanol concentrations and then critical point-dried. They were then mounted on aluminium stubs and gold-coated in an Emitech K550 (Emitech Ltd., Ashford, UK) sputter-coater before imaging by means of a scanning electron microscopy (EVO 50; ZEISS, Germany).

## 2.8. Immunofluorescence staining and confocal laser scanning microscope analysis

Cells grown on glass coverslips were fixed for 10 min at room temperature (RT) with 4% paraformaldehyde in 0.1M sodium phosphate buffer (PBS), pH 7.4. Briefly, hPDLSCs grown on Dual-Block sections were permeabilized with 0.5% Triton X-100 in PBS for 10 min, followed by blocking with 5% skimmed milk in PBS for 30 min. Primary monoclonal antibodies to anti-human vinculin (Santa Cruz Biotechnology, Santa Cruz, CA; USA) was used, followed by Alexa Fluor 488 green fluorescence conjugated goat anti-mouse as secondary antibodies (Molecular Probes, Invitrogen, Eugene, OR, USA). Subsequently, the sample was incubated with Alexa Fluor 594 phalloidin red fluorescence conjugate (1:500, Molecular Probes), as a marker of the actin cytoskeleton, and TOPRO for nuclei staining (1:100, Molecular Probes). Samples were visualized using a Zeiss (Jena, Germany) LSM510 META confocal system, connected to an inverted Zeiss Axiovert 200 microscope equipped with a Plan Neofluar oil-immersion objective (40×/1.3 NA). Images were collected using an argon laser beam with excitation lines at 488 nm and a helium-neon source (543 nm and 665 nm).

**2.9. Mineralization assay**

Mineralization in hPDLSC-cultures was determined by Alizarin Red S staining. The experiments were carried out in quadruplicate into a 6-well culture plate. Briefly cells from each patient were allowed to grow in basal (MSCM) or differentiation osteogenic (MSCM supplemented with hMSC Osteogenic single quotes) medium for 21 days with and without the collagenated Dual-Block biomaterial. Samples were fixed for 1h in 4% paraformaldehyde in 0.1M PBS, pH 7.4, washed three times with PBS (pH 7.4), then stained with 0.5% Alizarin Red S in H<sub>2</sub>O, pH 4.0, for 20 min at room temperature.

After staining, the cultures were washed three times with H<sub>2</sub>O followed by 70% ethanol.

For staining quantification of the mineralization process, samples were treated as previously described<sup>28</sup>. Briefly, 800µl 10 % (v/v) acetic acid were added to each well; cells were incubated for 30 min with shaking, then removed by scraping, transferred into a 1.5-mL vial and vortexed for 30 s. The obtained suspension was coated with 500 µl mineral oil (Sigma–Aldrich, St. Louis, MO, USA), heated to 85 °C for 10 min, then transferred to ice for 5 min, carefully avoiding the opening of the tubes until fully cooled, and centrifuged at  $20,000 \times g$  for 15 min. The samples were acidified (pH between 4.1 and 4.5) with 200 µl of 10 % (v/v) ammonium hydroxide. Aliquots (150 µl) were read in triplicate at 405 nm by a spectrophotometer ND-1000 NanoDrop Spectrophotometer (NanoDrop Technologies, Rockland, DE, USA).

## 2.10. Western Blot analysis

After three weeks of culture cells were lysated in RIPA buffer (1x PBS, 1% Igepal, 0.5% sodium deoxycholate, 0.1% sodium dodecyl sulphate (SDS) and 10µg/ml phenylmethylsulfonyl fluoride (PMSF), 10 µg/ml leupeptin and 10 µg /ml soybean trypsin inhibitor as inhibitors). The level of recovered protein was measured spectrometrically according to the instructions of the manufacturer using the Bio-Rad Protein Assay (detergent compatible) (Hercules, CA, USA).

Subsequently, 30µg of protein separated on SDS-PAGE, was transferred to nitrocellulose sheets using a semidry blotting apparatus. Sheets were saturated for 60 min at 37°C in blocking buffer (PBS supplemented with 5% skimmed milk), then incubated overnight at 4°C in blocking buffer containing primary antibodies such as:, collagen type I, and β-actin type I (Santa Cruz Biotechnology, Santa Cruz, CA, USA). They were incubated for 30 min at room temperature with HRP conjugated secondary

antibody diluted 1:5.000. Bands were visualized by the ECL method; using Alliance 2.7 (UVItect Limited, Cambridge, UK).

**2.11. SR X-ray phase contrast micro-CT**

The X-ray tomographic experiments were performed at the SYRMEP beamline (ELETTRA synchrotron light source, Trieste, Italy). The samples were investigated using isometric voxel with edge size of 9 μm; exposure time of 900 ms/projection; and X-ray beam energy of 16 keV, which was preliminarily found to provide acceptable imaging of both collagenated scaffold and cells while at the same time minimizing the thermal effect (reducing the absorption signal with energy increase). The sample-detector distance of 150 mm enabled to work in phase contrast mode with the typical edge enhancement feature.

The approach used in this work, i.e. phase-contrast in the edge enhancement regime, differs from conventional X-ray imaging because the resulting images are not based solely on attenuation contrast. The effect of an X-ray beam going through the sample is described by the refractive index,  $n(r) = 1 - \delta(r) + i\beta(r)$ , where  $\delta$  is the refractive index decrement and  $\beta$  is the attenuation index. As  $\delta$  is much larger than the imaginary part  $\beta$ , the phase approach provides greater sensitivity than the absorption approach.  $\delta$  is actually proportional to the mean electron density, which in turn is nearly proportional to the mass density.

The method used for quantitative volumetric reconstructions of the refractive index is based on a two-step approach: first, the phase projections are determined in the form of Radon projections (phase retrieval) and then the object function, i.e. the refractive index decrement  $\delta$ , is reconstructed by applying a conventional filtered back projection (FBP) algorithm.

Typically the phase retrieval implies the reconstruction of two different real-valued 3D distributions,  $\delta(r)$  and  $\beta(r)$ ; such reconstruction generally requires acquisition of at least two different 2D projections at each view angle. However, in some cases, it can be shown *a priori* that the distributions of the real and imaginary parts of the refractive index are proportional to each other, i.e.,  $\beta(r) = \varepsilon \delta(r)$ , where the proportionality constant  $\varepsilon$  does not depend on the spatial coordinates. This assumption is possible only for special classes of objects, such as *pure-phase* (i.e. very weakly absorbing) objects, or *homogeneous* objects, such as objects consisting predominantly of a single material (possibly, with a spatially varying density) (29). This last case is represented by our samples where, at the early stages of bone formation in the different culture medias, there is a slow variation of the complex amplitude (“monomorphous” specimen). In this situation, a single projection per each view angle is sufficient for reconstruction of the 3D distribution of the complex refractive index (30).

In this study, a phase-retrieval algorithm based on the Transport of Intensity equation (TIE) (29, 31) was applied to the acquired datasets with parameters tuned to edge enhancement reduction and balance noise minimization. Then the common filtered back-projection algorithm was used to reconstruct the slices. The X-TRACT software (CSIRO Mathematical and Information Sciences, Canberra, Australia) was applied for both the TIE-based phase retrieval and the reconstruction of X-ray phase-contrast slices. The different phases shown in the histogram, where the different grey values (proportional to  $\delta$ ) are reconstructed, were colored using a 3D display software to make them easier to distinguish. Volume rendering is a 3D visualization method by which data volumes are rendered directly, without the need for decomposition into geometric primitives. The commercial software VG Studio MAX 1.2 (Volume Graphics,



Heidelberg, Germany) was used to generate 3D images and visualize the phase distribution in 3D. Optimal image quality settings were obtained using the Scatter HQ algorithm with an oversampling factor of 5.0 and activated color rendering. X-ray contrast differences within samples translate into different peaks in the grey level scale, corresponding to the different phases. The volume of each phase is obtained by multiplying the volume of a voxel ( $\sim 730 \mu\text{m}^3$ ) by the number of voxels underlying the peak associated with the relevant phase. The Mixture Modeling algorithm (NIH ImageJ Plugin) was implemented to threshold the histograms. Thresholded slices were used to automatically separate the new cell-derived phase from the scaffold phase. The threshold of the newly formed phase (mineralized bone) was  $\sim 115$ .

A structural analysis of the trabecular structure (including scaffold and newly formed bone phases) was performed in order to verify if hPDLSC-culture in the two medias induced morphometric modification of the templates. The following morphometric parameters were evaluated: Anisotropy Degree (DA); Connectivity Density, i.e. number of trabeculae per unit volume (Conn.D. – expressed in  $\text{pixel}^{-3}$ ); Mean Trabecular Thickness (TbTh - expressed in micrometers); Mean Trabecular Separation (TbSp - expressed in micrometers); Mean Trabecular Number (TbNr – per millimeter); Sample Volume (SV) to Total Volume (TV) ratio (SV/TV – expressed as a percentage).

The Degree of Anisotropy (DA) is a measure of how highly oriented the substructures are within a certain volume. Trabecular structure could vary its orientation depending on hPDLSC-culture and can become anisotropic. We used the mean intercept length (MIL) method for determining anisotropy (32, 33). DA is calculated as  $1 - \text{length of the shortest axis} / \text{length of the longest axis}$ , resulting in  $0 = \text{fully isotropic structure}$ ;  $1 = \text{fully anisotropic structure}$ .

## 2.12. Data and statistical analysis

Statistical analysis was performed using Graph Pad Prism 4 (Graph Pad Software Inc., San Diego, CA, USA). The results were presented as means  $\pm$  standard errors of the mean (SEM). Groups of data were compared with analysis of variance (two-way ANOVA) followed by Tukey's multiple comparison tests. P values  $\leq 0.05$  were considered statistically significant.

## 3. Results

### 3.1. Cells culture

*In vitro* cell cultures are an ideal tool to investigate and compare different biomaterial scaffolds; in this context the current study assessed the cellular response to 3-D Dual-Block biomaterial.

Human PDLSCs used in this experimental protocol exhibited a cell-surface stem cell antigen phenotype positive for CD29, CD90, CD44, CD73, CD105, CD146, CD166, Oct 3/4, HLA-ABC, Sox-2 and SSEA-4 (Figure 1, section A). The proliferation rate and viability of the hPDLSCs was investigated performing an MTT and Trypan Blue exclusion test at 24, 48, 72h and 1 week of culture. Both analyses showed that the cells seeded on the dual-block showed a slightly lower growth at all examined time-points (Figure 1, section B and C).

### 3.2. Morphological analysis

SEM observations facilitated to clarify the performance of the cells/ biomaterial construct. Scanning electron microscopy (SEM) morphological analysis of Dual Block was carried out before hPDLSCs seeding. The biomaterial exhibited the characteristic

aspect represented by cortical bone anchored to cancellous bone (Figure 2, section A). The commercially biomaterial block is shown in the inset of the Figure 2 (section A1). Primary hPDLSCs cells, exhibiting long processes and fibroblast-like morphology, were evident at ultrastructural level (Figure 2, section B). After 24 h of incubation in presence of the biomaterial no significant difficulty in the adhesiveness process was evident, in fact a confluent cellular multilayer adhering directly on the cortical and cancellous biomaterial confirmed the high biocompatibility of the analyzed scaffold (Figure 2, section C).

At higher magnification, contact zone established through extending cytoplasmic processes and filopodia, which enabled the anchorage of the cells, was shown; the distal end of the filopodia and cytoplasmic processes were directly associated with the constituent part of the biomaterial (Figure 2, section D). The immunohistochemistry results showed that a specific positivity to vinculin was present on 3D scaffold indicating an intimate contact between cells and biomaterial (Figure 2, section E, F, G and H).

**3.3. Osteogenic Differentiation**

At 21 days of culture the observation of cells stained with Alizarin Red S, revealed newly deposited bone in Diff@group (Figure 3, section A2). In presence of biomaterial a strong osteogenic induction was present in both DB-ctrl@group ad DB-Diff@group (Figure 3, section B1 and 2). The sensitivity of the colorimetric method obtained by the extraction of the calcified mineral at low pH, permitted to evidence an intense staining peak in both undifferentiated and differentiated cells seeded on 3D biomaterial (Figure 3, section C).

Western blot analysis showed in cells induced to osteogenic differentiation and hPDLSCs seeded on biomaterial an up-regulation of collagen type I, a bone tissue-specific protein, demonstrating an evident maturation of bone cells (Figure 3, section D). Densitometric analysis confirmed the results obtained by western blot investigation (Figure 3, section E).

### 3.4. Micro-CT

The osteogenic potential of collagenated porcine dual-blocks cultured with hPDLSCs, statistically demonstrated by Alizarin Red S, Western blot and densitometric analysis, was validated by the quantitative data extracted by the 3D micro-CT analysis. Micro-CT was able to easily distinguish in 3D the newly formed bone phase from the collagenated porcine scaffold. Cell-medium-scaffold interactions modified the scaffold structure, thus producing images in which two different phases with different refractive index were evident. Results are given for both basal (DB-ctrl; figure 4) and differentiating (DB-Diff; figure 5) media. The scaffold and the newly formed bone were colored using 3D display software to make them more easily recognizable. The scaffold structure was shown in white (figure 4-5, panels A and D), while the newly formed bone (produced by the cells grown on the bioscaffold) was depicted in magenta (figure 4-5, panels B and E).

While micro-CT revealed that no significant (detectable) bone regeneration was present after the first week in both basal and differentiating media (data not shown), starting from the second week of culture the magenta phase is easily recognizable in all the scaffolds, both in basal (figure 4, panels B and E) and differentiating (figure 5, panels B and E) media. This phase seems to occur preferentially in the trabecular portion, being

probably due to the higher porosity of the scaffold in this site with respect to the compact areas.

A relevant quantitative result is the decrease of the cultured scaffolds mass density ( $\rho$ , expressed in  $\text{mg}/\text{cm}^3$ ) from the first to the second week of culture, while a slight increase was observed from the second to the third week. Such evidence is observed independently if the culture is in basal (DB-ctrl) or in differentiating (DB-Diff) medium and it is confirmed by the profile of the “Intensity Counts vs. Grey Level” for the DB-ctrl (figure 6a) and the DB-diff (figure 6b) cultures. Indeed, due to the experimental phase-contrast set-up and the TIE algorithm implemented for the data analysis, the grey levels - here referred to an unsigned 8-bit scale - are proportional to the refractive index decrement  $\delta$ , that in turn is nearly proportional to the mass density  $\rho$  of the collagenated porcine scaffold.

The amount of the newly formed bone (magenta phase in figure 4, panels B and E and figure 5, panels B and E) was calculated by counting the corresponding voxels underlying the peak associated with the relevant phase. The Mixture Modeling algorithm (NIH ImageJ Plugin) was implemented to threshold the histograms and to automatically separate the new bone from the scaffold phase. The obtained data were expressed as BV/TV (%), i.e. the volume ratio of the newly-formed bone structure (BV) to the total construct volume (TV). The BV/TV ratio is reported in the top-right insert of the figure 6C as a function of time from PDLSCs seeding onto the scaffold. Interestingly, a comparison between the culture in basal medium (DB-ctrl) and in differentiating medium (DB-diff) showed, within the limits of the sample size, that the BV/TV ratio in differentiating medium is almost 7-fold greater than in basal medium after 2 weeks of culture and more than 10-fold greater after 3 weeks of culture.

1  
2  
3  
4 The color map of the newly-formed bone thickness distribution confirmed significantly  
5 lower BV/TV percentages in cultures in basal medium (Figure 4, panels C and F) with  
6 respect to those in differentiating medium (Figure 5, panels C and F). It also showed  
7 that the compact region of the scaffolds is partially mineralized only in differentiating  
8 medium, further demonstrating the differentiating process acceleration of the hPDLSCs  
9 in the DB-diff@group, with respect to the DB-ctrl@group.

10  
11 To investigate more deeply the newly formed bone changes in time, the bone thickness  
12 distribution vs. the bone volume normalized to the total sample volume was also  
13 assessed. Histograms of the distribution of the bone thickness in all the investigated  
14 samples are reported in Figure 6, panel C. It is shown here that while the average bone  
15 thickness was  $\sim 130 \mu\text{m}$  in cultures made in differentiating medium, none bone  
16 formation reached this thickness in basal medium, even after three weeks of culture.

17  
18 A structural analysis was also performed on the spongy portion of the samples in order  
19 to verify if hPDLSC-culture in the two media induced morphometric modification of  
20 the scaffold templates. The results are reported in Figure 7. The kinetics curve presents  
21 a comparable behavior in basal and differentiating media for all the morphometric  
22 parameters considered. Furthermore, with the exclusion of the DA parameter that seems  
23 not varying significantly ( $p > 0.05$ ) in time (presenting values between 0.6 and 0.8),  
24 significant differences ( $p < 0.05$ ) were observed between the first and the second week  
25 of culture in terms of Conn.D., TbTh and SV/TV parameters, that significantly  
26 increased, and for the TbSp parameter, that consistently decreased. This evidence  
27 further demonstrates that a significant mineralization appears starting from the 2<sup>nd</sup> week  
28 of culture, as previously stated by cell staining with Alizarin red S (Figure 3C) and  
29 validated by micro-CT (Figure 4 and Figure 5).

30  
31  
32  
33  
34  
35  
36  
37  
38  
39  
40  
41  
42  
43  
44  
45  
46  
47  
48  
49  
50  
51  
52  
53  
54  
55  
56  
57  
58  
59  
60

4. Discussion

A critical goal in tissue engineering is to obtain scaffolds with tailored physical, mechanical and biological properties to act as template for stem cell growth, proliferation and differentiation in newly formed bone (34). The choice of the best scaffold-culture medium matching is a major issue in order to mimic ECM architecture and biological functions. In fact scaffolds are not only required to provide mechanical support, but they are asked to carry inductive molecules, cells and supply signals to control the structure and the function of the newly formed bone. Cell adhesion to the substrate is necessary for good scaffold-cell interactions and must occur before cell spreading, division and differentiation (11, 35).

This paper presents the characterization of early-stage *in vitro* bone formation on collagenated porcine Dual-block scaffolds seeded with PDL stem cells and cultured in basal or differentiating media. Morphological analyses by light and scanning electron microscopy explained the performance of cells in contact with the collagenated Dual Block biomaterial. The analysis showed cellular proliferation of the hPDLSCs seeded on scaffold and subsequent colonization of the biomaterial. We got evidence that cells adhered to the uppermost surface of the scaffold, also establishing cellular bridges and organizing a network between the cancellous spaces. To validate the performance of the biomaterial we have explored the focal adhesion area evaluating the vinculin expression trough confocal laser scanning microscopy. Previously fluorescently-tagged vinculin has been used to demonstrate that the surface features of biomaterials made of either titanium or stainless steel are critical for number, size and dynamics of focal adhesions (36) and that the focal adhesion area increases in osteogenic cells (37). In PDLSCs

several anchoring junctions bind cells to the substrate, indicating the performance of above-mentioned biomaterials.

Alizarin Red S showed a mineralized extracellular matrix in presence of the scaffold both in control (DB-ctrl) and, in particular in differentiating (DB-diff) cultures, indicating that the collagenated Dual- Block offers an adequate support for tissue reconstruction due to its biological characteristics and ability to support cell growth and differentiation. The progression of osteogenic differentiation is indicated by bone-related proteins, in particular collagen type 1; the upregulation of this protein in DB-ctrl cells can give insights that the scaffold could be designed as co-protagonist of the cells in differentiation process (7).

The study is supported and validated by a demonstrative application of SR X-ray phase contrast micro-CT. This analysis disclosed spotted bone deposits, detected from the second week of culture in both media, onto the scaffold template with high resolution and in 3D. BV/TV ratio in differentiating medium was found to be almost 7-fold greater than in basal medium after 2 weeks of culture and more than 10-fold greater after 3 weeks of culture. The poor signal in the basal medium may be due to the fact that here the cells take longer time to differentiate than in differentiating medium even if the osteoinductive potential is preserved. This is also confirmed by the morphometric analysis performed in the spongy volume of the samples.

Interestingly, micro-CT studies revealed a mass density decrease of the scaffolds seeded with hPDLSCs in both media from the first to the second week of culture, while a slight increase was observed from the second to the third week. This seems to indicate that the scaffold bioresorption is more accentuated up to the second week of culture. Anyhow looking at scaffold changes over time is a still challenging subject and needs a



statistically consistent sample and proper boundary conditions. More powerful detection systems are needed to investigate larger scaffolds preserving and possibly increasing the spatial resolution (11). This will provide reliable quantitative data when micro-CT reconstructions of biostructures undergoing remodeling (like during cell adhesion, proliferation and differentiation on a bioresorbable scaffold) require segmentation.

Notably, absorption-based micro-CT is not recommended for analysis of the present samples, due to low X-ray absorption by collagenated scaffolds (14). Our demonstrative experiments were indeed conducted on single sample-detector distance, with a phase-contrast set-up and subsequent application of a phase retrieval algorithm based on the Transport of Intensity equation (TIE). The chosen method was proved to successfully reconstruct the distribution of  $\delta$  in our samples that, at the early stages of bone formation in the different culture medias, can be considered “monomorphous” (i.e. collagenated) specimens.

In conclusion, this paper describes and demonstrates the osteogenic potential of collagenated porcine dual-blocks cultured with periodontal ligament stem cells and shows the feasibility of SR phase-contrast micro-CT analysis to study newly bone formation on collagenated bioscaffolds. More generally, it provides clear evidence that the non-invasive and quantitative micro-CT may be an important characterization tool for bone engineering approaches.

**Acknowledgements**

The authors acknowledge the ELETTRA User Office for kindly providing beam-time, Dr. Timur Gureyev, Senior Principal Research Scientist at CSIRO Materials Science and Engineering (AUSTRALIA) for his fundamental suggestions during X-TRACT

data analysis and Dr Ilaria Merciaro for experimental procedure on cell culture (Department of Medical, Oral and Biothechnological Sciences, Chieti, Italy).

This work arises from a collaboration between COST NAMABIO partners (A.M., A.G., S.M., and A.P.) and was financed from the Program PRIN funds of Ministero dell'Istruzione, Università e Ricerca (Prot. 20102ZLNJ5).

Manuscript proof

References

[1] Disa JJ, Cordeiro PG. Mandible reconstruction with microvascular surgery. 2000; 19(3):226-34.

[2] Emerick KS, Teknos TN. State-of-the-art mandible reconstruction using revascularized free-tissue transfer. Expert Rev Anticancer Ther 2007; 7(12): 1781–1788.

[3] Ward BB, Brown SE, Krebsbach PH. Bioengineering strategies for regeneration of craniofacial bone: a review of emerging technologies. Oral Diseases 2010; 16(8): 709–716.

[4] Giuliani A, Manescu A, Langer M, et al. Three years after transplants in human mandibles, histological and in-line HT revealed that stem cells regenerated a compact rather than a spongy bone: biological and clinical implication. Stem Cells Transl Med 2013; 2(4): 316-324.

[5] Huang GT, Gronthos S, Shi S. Mesenchymal stem cells derived from dental tissues vs. those from other sources: their biology and role in regenerative medicine. J Dent Res 2009; 88(9): 792-806.

[6] Eleuterio E, Trubiani O, Sulpizio M, et al. Proteome of human stem cells from periodontal ligament and dental pulp. Plos One 2013; 8(8): e7101.

[7] Trubiani O, Fulle S, Traini T, et al. Functional assay, expression of growth factors and proteins modulating bone-arrangement in human osteoblasts seeded on an anorganic bovine bone biomaterial. Eur Cell Mater 2010 Jul 21; 20:72-83.

[8] Yang H, Gao LN, An Y, et al. Comparison of mesenchymal stem cells derived from gingival tissue and periodontal ligament in different incubation conditions. Biomaterials 2013; 34(29): 7033-47.

- [9] Trubiani O, Orsini G, Zini N, et al. Regenerative potential of human periodontal ligament derived stem cells on three-dimensional biomaterials: a morphological report. *J Biomed Mater Res A*. 2008; 87(4): 986-93.
- [10] Trubiani O, Zalzal SF, Paganelli R, et al. Expression profile of the embryonic markers nanog, OCT-4, SSEA-1, SSEA-4, and frizzled-9 receptor in human periodontal ligament mesenchymal stem cells. *J Cell Physiol*. 2010; 225(1): 123-31.
- [11] Giuliani A, Moroncini F, Mazzoni S, et al. Polyglycolic Acid-Polylactic Acid scaffold response to different progenitor cell in vitro cultures: a demonstrative and comparative X-Ray Synchrotron Radiation Phase-Contrast Microtomography study. *Tissue Eng Part C Methods*. 2014 Apr; 20(4):308-16.
- [12] Gomes ME, Bossano CM, Johnston CM, et al. In Vitro Localization of Bone Growth Factors in Constructs of Biodegradable Scaffolds Seeded with Marrow Stromal Cells and Cultured in a Flow Perfusion Bioreactor. *Tissue Eng* 2006; 12(1), 177-188.
- [13] Rada T, Reis RL, Gomes ME. Adipose Tissue-Derived Stem Cells and Their Application in Bone and Cartilage Tissue Engineering. *Tissue Eng Part B* 2009; 15(2), 113-125.
- [14] Giuliani A, Fiori F, Manescu A, et al. Synchrotron Radiation and Nanotechnology for Stem Cell Research. In Ali Gholamrezanezhad eds. *Synchrotron Radiation and Nanotechnology for Stem Cell Research. Stem Cells in Clinic and Research*. InTech 2011, Rijeka, Croatia, 683-708.
- [15] Moon SU, Kim J, Bokara KK, et al. Carbon nanotubes impregnated with subventricular zone neural progenitor cells promotes recovery from stroke. *Int J Nanomedicine* 2012; 7: 2751–2765.

[16] Belicchi M, Cancedda R, Cedola A, et al. Some applications of nanotechnologies in stem cells research. *Mater Sci Eng B* 2009; *Solid State Mater Adv Technol* 165(3), 139-147.

[17] Cancedda R, Cedola A, Giuliani A, et al. Bulk and interface investigations of scaffolds and tissue-engineered bones by X-ray microtomography and X-ray microdiffraction. *Biomaterials* 2007; 28(15): 2505-2524.

[18] Renghini C, Giuliani A, Mazzoni S, et al. Microstructural characterization and in vitro bioactivity of porous glass-ceramic scaffolds for bone regeneration by synchrotron radiation X-ray microtomography. *J Eur Ceram Soc* 2013; 33(9): 1553- 1565.

[19] Cancedda R, Dozin B, Giannoni P, Quarto R. Tissue engineering and cell therapy of cartilage and bone. *Matrix Biol* 2003; 22(1): 81-91.

[20] Ohgushi H, Tamai S, Dohi Y, et al. In vitro bone formation by rat marrow cell culture. *J. Biomed. Mater. Res.* 1996; 32(3): 333–340.

[21] Giuliani A, Manescu A, Larsson E, et al. In Vivo Regenerative Properties of Coralline-Derived (Biocoral) Scaffold Grafts in Human Maxillary Defects: Demonstrative and Comparative Study with Beta-Tricalcium Phosphate and Biphasic Calcium Phosphate by Synchrotron Radiation X-Ray Microtomography. *Clin Implant Dent Relat Res.* 2013.doi: 10.1111/cid.12039. [Epub ahead of print]

[22] Gigante A, Busilacchi A, Lonzi B, et al. Purified collagen I oriented membrane for tendon repair: An ex vivo morphological study. *J. Orthop. Res.*2013; 31(5): 738–745.

[23] Arfelli F, Assante M, Bonvicini V, et al. Low-dose phase contrast X-ray medical imaging. *Phys Med Biol* 1998; 43(10), 2845–2852.

[24] Wu X, Yan A. Phase retrieval from one single phase contrast x-ray image. *Opt. Express* 2009; 17(13), 11187.

- [25] Hofmann R, Moosmann J, Baumbach T. Criticality in single-distance phase retrieval, *Opt. Express* 2011; 19(27), 25881–25890.
- [26] Langer M, Cloetens P, Peyrin F. Fourier-wavelet regularization of phase retrieval in x-ray in-line phase tomography, *J. Opt. Soc. Am. A* 2009; 26(8), 1876-1881.
- [27] Carranza FA. The Tooth-Supporting Structures. In: Newmann, editor. *Clinical Periodontology* 1996. Philadelphia: W. B. Saunders, 31-50.
- [28] Gregory CA, Gunn WG, Peister A, Prockop DJ. An Alizarin red-based assay of mineralization by adherent cells in culture: comparison with cetylpyridiniumchloride extraction. *Anal Biochem.* 2004; 329(1):77-84.
- [29] Gureyev TE, Pogany A, Paganin DM, Wilkins SW. Linear algorithms for phase retrieval in the Fresnel region, *Opt Commun* 2004; 231(1-6), 53–70.
- [30] Gureyev TE, Paganin DM, Myers GR, et al. Phase-and-amplitude computer tomography, *Appl Phys Lett* 2006; 89(3), 034102.
- [31] Gureyev TE, Mayo SC, Myers DE, et al. Refracting Röntgen's rays: Propagation-based x-ray phase contrast for biomedical imaging. *J Appl Phys* 2009; 105(10), 102005.
- [32] Harrigan TP, Mann RW. Characterization of microstructural anisotropy in orthotropic materials using a second rank tensor. *J Mater Sci* 1984; 19(3): 761-767.
- [33] Odgaard A. Three-dimensional methods for quantification of cancellous bone architecture. *Bone* 1997; 20(4): 315-28.
- [34] Causa F, Netti PA, Ambrosio LA. Multi-functional scaffold for tissue regeneration: the need to engineer a tissue analogue. *Biomaterials* 2007; 28(34): 5093-9.
- [35] Davies JE, Causton B, Bovell Y, et al. The migration of osteoblasts over substrata of discrete surface charge. *Biomaterials* 1986; 7(3): 231-233.

1  
2  
3  
4  
5  
6  
7  
8  
9  
10  
11  
12  
13  
14  
15  
16  
17  
18  
19  
20  
21  
22  
23  
24  
25  
26  
27  
28  
29  
30  
31  
32  
33  
34  
35  
36  
37  
38  
39  
40  
41  
42  
43  
44  
45  
46  
47  
48  
49  
50  
51  
52  
53  
54  
55  
56  
57  
58  
59  
60

[36] Diener A, Nebe B, Luthen F, et al. Control of focal adhesion dynamics by material surface characteristics. *Biomaterials* 2005; 26(4): 383-392.

[37] Born AK, Rottmar M, Lischer S, et al. Correlating cell architecture with osteogenesis: first steps towards live single cell monitoring. *Eur Cell Mater* 2009; 18: 49-62.

Manuscript proof

## Figure Captions

Figure 1. Cytofluorimetric analysis of hPDLSCs culture. The values are expressed as mean fluorescence ratio (MFI) obtained dividing the MFI of positive events by the MFI of negative events. In section A the numeric values of MFI ratio are the mean  $\pm$  standard deviation (SD) of three separate experiments using cells at 2nd passage.

MTT assay in hPDLSCs grown in vitro under undifferentiating condition, with (DB-ctrl@group) or without biomaterial (ctrl@group), over 24h, 48h, 72h, 1 week time-points. The proliferation rate was measured as the absorbance detected at 490 nm.

Trypan blue exclusion test show the proliferation rate and viability of hPDLSCs. In both tests MTT (B) and Trypan Blue (C) the cells seeded on the dual-block showed a slightly lower growth in all examined time-points. The Y-axis shows cell number, and X-axis shows culture time. Results are expressed as mean  $\pm$ SEM of three independent experiments for each patient.

Figure 2. Scanning electron microscopy of Dual Block before grafting. (A) The cortical bone is anchored to cancellous bone; the biomaterial block, as commercially provided, is showed in the inset (A1). (B) Photomicrograph of a primary culture of human Periodontal Ligament Stem Cell (hPDLSC) line expanded ex vivo; it shows a morphological homogeneous fibroblast-like appearance with a stellate shape and elongated cytoplasmic processes. (C) Living un-induced hPDLSCs (DB-ctrl@group), after 24h of culture, grown on tridimensional scaffold. High magnification revealed hPDLSCs adhesion to substrate: in fact, confluent cells were observed on the biomaterial surface. (D) Cellular margin were indiscernible for the intimate contact



between neighboring cells; cellular bridge was evident in the cancellous space. (E-H) Representative image of hPDLSCs seeded on 3D-biomaterial expressing vinculin and actin. Section E (green fluorescence) showed a punctate vinculin labelling in cells adhering to substrate. Rhoadamine –Phalloidin staining showed the spatial cytoskeleton of human periodontal ligament stem cells (red fluorescence, F). In section G it was possible to observe the nuclei stained with Topro (blue fluorescence). Section H indicated merged image with the triple staining of cells seeded on biomaterial. Asterisk: 3D-Dual Block.

Figure 3. The osteogenic differentiation of hPDLSCs was evaluated as extracellular matrix mineralization for 21 day, in basal (A1 and B1) and osteogenic medium (A2 and B2), in absence (A) or presence (B) of the collagenated biomaterial. If a mineralized matrix is present in osteogenic induced cells (A2) also in absence of the scaffold, an evident mineralization was detected both in basal conditions (B1) and in osteogenic induction (B2) when the scaffold is present.

Mineralization of hPDLSCs, grown for 1, 2 and 3 wks under osteogenic and basal conditions, with or without biomaterial, was evaluated by cell staining with Alizarin red S (ARS) and quantification of staining (C) via extraction with ammonium hydroxide at different commitment time. The amount of released dye is measured by a microplate reader at 405 nm. The values, expressed as units of optical density (O.D.), are the mean  $\pm$  SEM of three independent experiments, in which different cell samples were used. Immunoblotting experiments and densitometric analysis of collagen type 1 showed an upregulation of protein in osteogenic induced cells respect to control. In DB-ctrl@group a quantity of the collagen type 1 protein similar to DB-diff@group was present

indicating the osteoinductive properties of the biomaterial. B-actin represents an housekeeping protein (D and E).

Figure 4. Dual block and hPDLSCs in basal medium. The interaction between cells and scaffold produces 3D Micro-CT images with two different phases, corresponding to different  $\delta$  (refractive index decrement) values. DB scaffolds are rendered in grey (panels a, b at wk2; panels d, e at wk3), whereas the contrast produced by cells - the newly-formed bone - is colored in magenta (panel b at wk2; panel e at wk3). Color map of bone thickness distribution at wk2 and wk3 are given in panel c and panel f, respectively. Thickness scale on the left. Bar: 500  $\mu\text{m}$ .

Figure 5. Dual block and hPDLSCs in osteogenic medium. The interaction between cells and scaffold produces 3D Micro-CT images with two different phases, corresponding to different  $\delta$  (refractive index decrement) values. DB scaffolds are rendered in grey (panels a, b at wk2; panels d, e at wk3), whereas the contrast produced by cells - the newly-formed bone - is colored in magenta (panel b at wk2; panel e at wk3). Color map of bone thickness distribution at wk2 and wk3 are given in panel c and panel f, respectively. Thickness scale on the left. Bar: 500  $\mu\text{m}$ .

Figure 6. (a-b) Portion of the profile of the Intensity Counts vs. Grey Levels (proportional to the refractive index decrement  $\delta$ ). The integrated areas of the represented peaks correspond to the collagenated porcine Dual-block volume in scaffolds cultured in basal medium (panel a) and differentiating medium (panel b). In both media the contrast produced at wk2 of culture is lower than for wk1, but increases

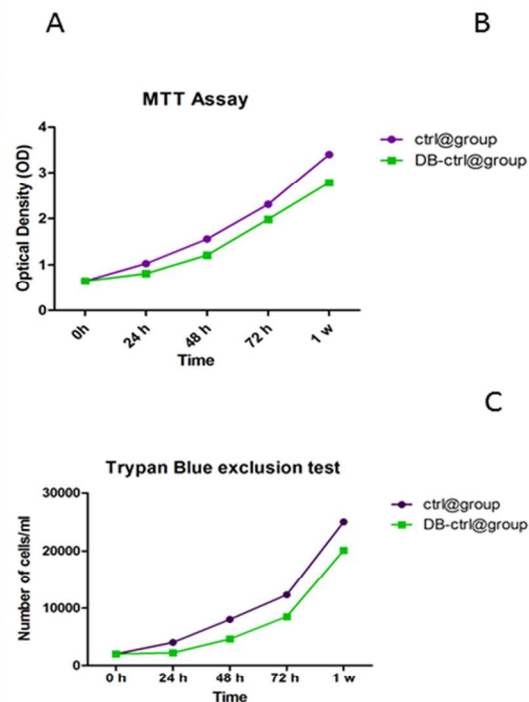
1  
2  
3  
4  
5  
6  
7  
8  
9  
10  
11  
12  
13  
14  
15  
16  
17  
18  
19  
20  
21  
22  
23  
24  
25  
26  
27  
28  
29  
30  
31  
32  
33  
34  
35  
36  
37  
38  
39  
40  
41  
42  
43  
44  
45  
46  
47  
48  
49  
50  
51  
52  
53  
54  
55  
56  
57  
58  
59  
60

from wk2 to wk3. (c) Histograms of the distribution of the bone thickness in all the investigated samples at wk2 and wk3 of culture. The volume ratio ( $= BV/TV$ ) of the newly-formed bone structure (BV) to the total construct volume (TV) is reported in the top-right insert.

Figure 7. Morphometric parameters investigated in scaffolds cultured with hPDLSCs, both in basal and differentiating media, after 1, 2 and 3 wks of culture: Anisotropy Degree (DA); Connectivity Density (Conn.D. – expressed in  $\text{pixel}^{-3}$ ); Mean Trabecular Thickness (TbTh - expressed in micrometers); Mean Trabecular Separation (TbSp - expressed in micrometers); Mean Trabecular Number (TbNr – per millimeter); Sample Volume (SV) to Total Volume (TV) ratio (SV/TV – expressed as a percentage).

Flow cytometry hPDLSCs		
Antigens		MFI Ratio $\pm$ SD
CD13	+	8,3 $\pm$ 3,5
CD14	-	1,4 $\pm$ 0,2
CD29	++	62,9 $\pm$ 3,2
CD34	-	1,4 $\pm$ 0,2
CD44	++	24,5 $\pm$ 2,3
CD45	-	1,4 $\pm$ 0,3
CD73	++	41,7 $\pm$ 3,4
CD90	+++	160,1 $\pm$ 15,6
CD105	+	25,5 $\pm$ 2,3
CD117	+/-	4,2 $\pm$ 0,8
CD133	-	2,1 $\pm$ 0,4
CD144	-	1,2 $\pm$ 0,1
CD146	+	11,5 $\pm$ 1,3
CD166	+	8,4 $\pm$ 0,6
CD271	-	1,3 $\pm$ 0,3
HLA-ABC	+++	121,3 $\pm$ 18,2
HLA-DR	-	1,1 $\pm$ 0,1
OCT3/4	+	37,6 $\pm$ 0,4
Sox-2	+++	103,2 $\pm$ 7,9
SSEA-4	++	33,6 $\pm$ 2,7

- negative expression; +/- low expression; + moderate expression; ++ positive; +++ high expression; MFI Ratio is the average of five different biological samples  $\pm$  standard deviation; Cutoff Ratio positivity >2.0.

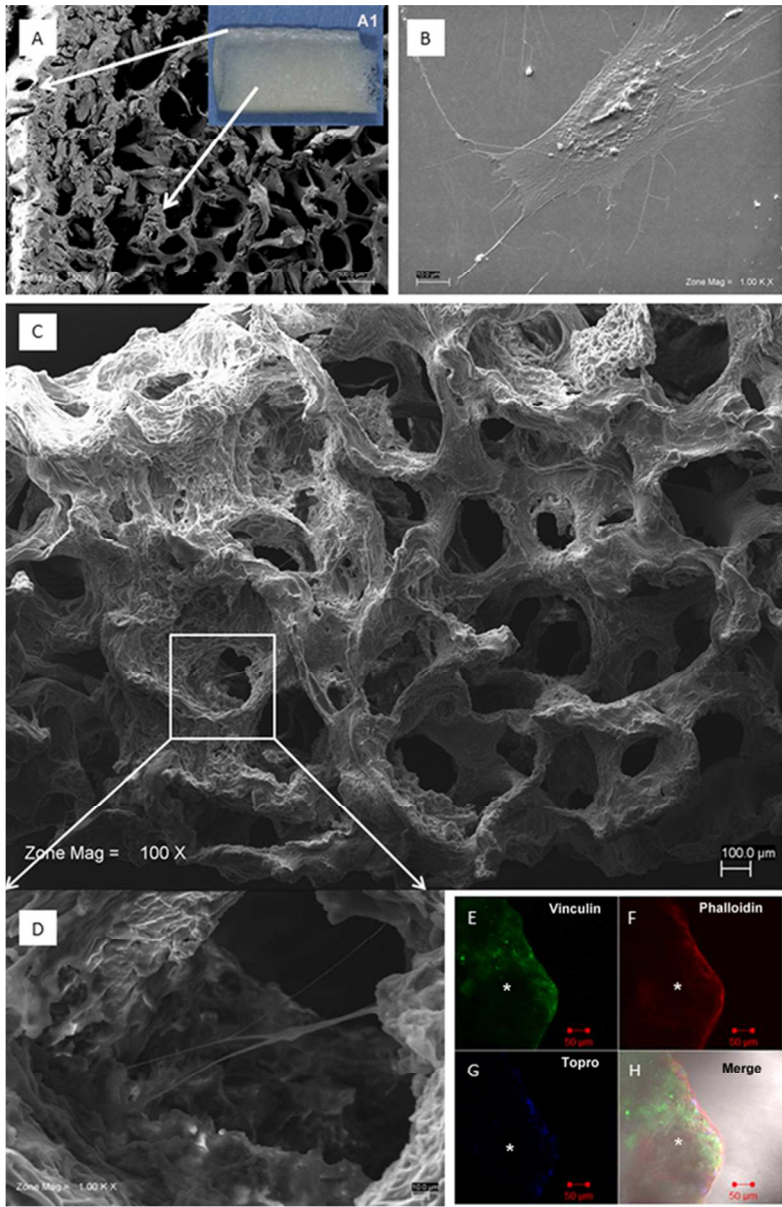


Cytofluorimetric analysis of hPDLSCs culture. The values are expressed as mean fluorescence ratio (MFI) obtained dividing the MFI of positive events by the MFI of negative events. In section A the numeric values of MFI ratio are the mean  $\pm$  standard deviation (SD) of three separate experiments using cells at 2nd passage.

MTT assay in hPDLSCs grown in vitro under undifferentiating condition, with (DB-ctrl@group) or without biomaterial (ctrl@group), over 24h, 48h, 72h, 1 week time-points. The proliferation rate was measured as the absorbance detected at 490 nm.

Trypan blue exclusion test show the proliferation rate and viability of hPDLSCs. In both tests MTT (B) and Trypan Blue (C) the cells seeded on the dual-block showed a slightly lower growth in all examined time-points. The Y-axis shows cell number, and X-axis shows culture time. Results are expressed as mean  $\pm$  SEM of three independent experiments for each patient.

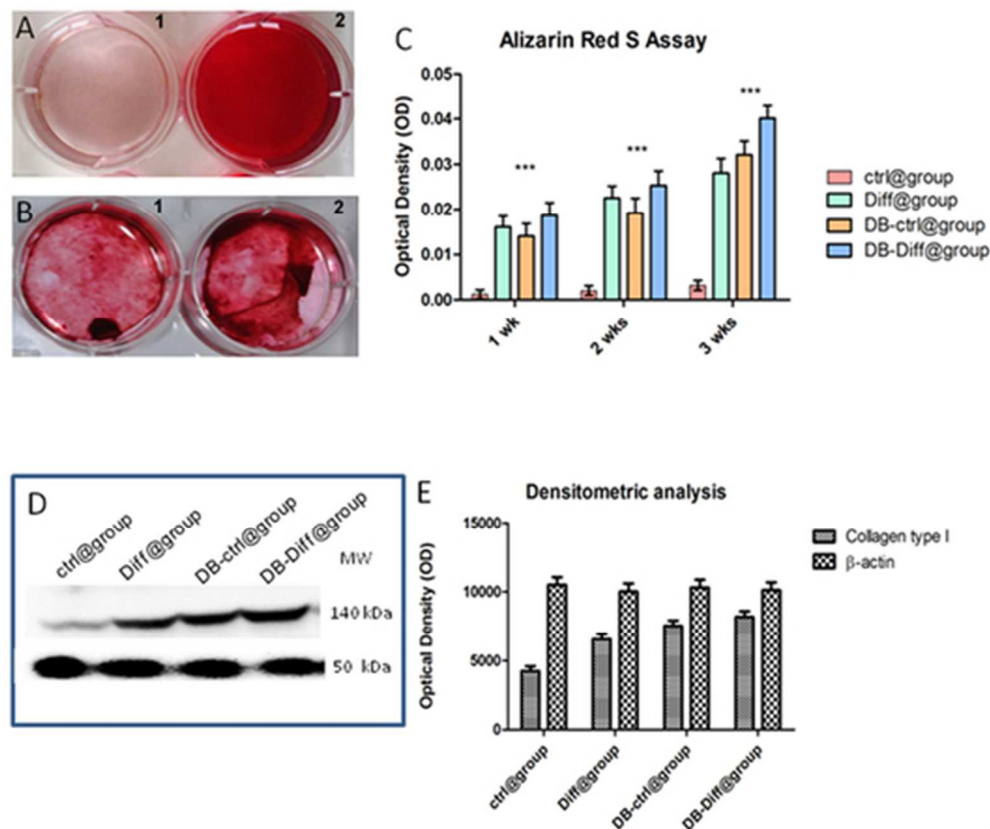
88x69mm (300 x 300 DPI)



Scanning electron microscopy of Dual Block before grafting. (A) The cortical bone is anchored to cancellous bone; the biomaterial block, as commercially provided, is showed in the inset (A1). (B) Photomicrograph of a primary culture of human Periodontal Ligament Stem Cell (hPDLSC) line expanded ex vivo; it shows a morphological homogeneous fibroblast-like appearance with a stellate shape and elongated cytoplasmic processes. (C) Living un-induced hPDLSCs (DB-ctrl@group), after 24h of culture, grown on tridimensional scaffold. High magnification revealed hPDLSCs adhesion to substrate: in fact, confluent cells were observed on the biomaterial surface. (D) Cellular margin were indiscernible for the intimate contact between neighboring cells; cellular bridge was evident in the cancellous space. (E-H) Representative image of hPDLSCs seeded on 3D-biomaterial expressing vinculin and actin. Section E (green fluorescence) showed a punctate vinculin labelling in cells adhering to substrate. Rhodamine-Phalloidin staining showed the spatial cytoskeleton of human periodontal ligament stem cells (red fluorescence, F). In section G it was possible to observe the nuclei stained with Topro (blue fluorescence). Section H indicated merged image with the triple staining of cells seeded on biomaterial. Asterisk: 3D-Dual Block.

54x83mm (300 x 300 DPI)

Manuscript proof



The osteogenic differentiation of hPDLSCs was evaluated as extracellular matrix mineralization for 21 day, in basal (A1 and B1) and osteogenic medium (A2 and B2), in absence (A) or presence (B) of the collagenated biomaterial. If a mineralized matrix is present in osteogenic induced cells (A2) also in absence of the scaffold, an evident mineralization was detected both in basal conditions (B1) and in osteogenic induction (B2) when the scaffold is present.

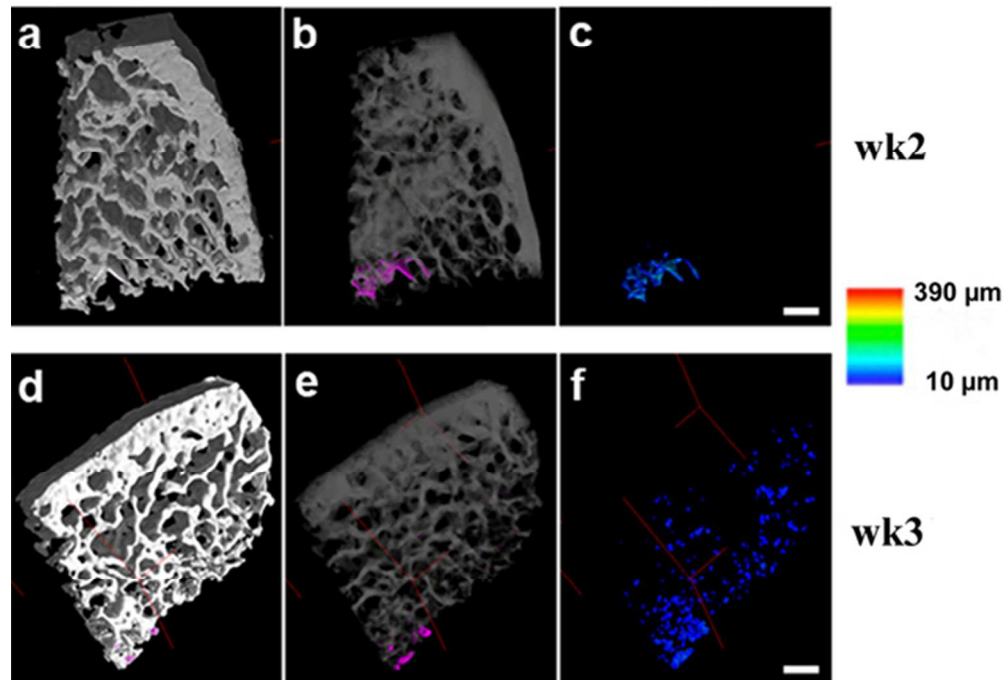
Mineralization of hPDLSCs, grown for 1, 2 and 3 wks under osteogenic and basal conditions, with or without biomaterial, was evaluated by cell staining with Alizarin red S (ARS) and quantification of staining (C) via extraction with ammonium hydroxide at different commitment time. The amount of released dye is measured by a microplate reader at 405 nm. The values, expressed as units of optical density (O.D.), are the mean  $\pm$  SEM of three independent experiments, in which different cell samples were used.

Immunoblotting experiments and densitometric analysis of collagen type 1 showed an upregulation of protein in osteogenic induced cells respect to control. In DB-ctrl@group a quantity of the collagen type 1 protein similar to DB-diff@group was present indicating the osteoinductive properties of the biomaterial.  $\beta$ -actin represents an housekeeping protein (D and E).

45x38mm (300 x 300 DPI)



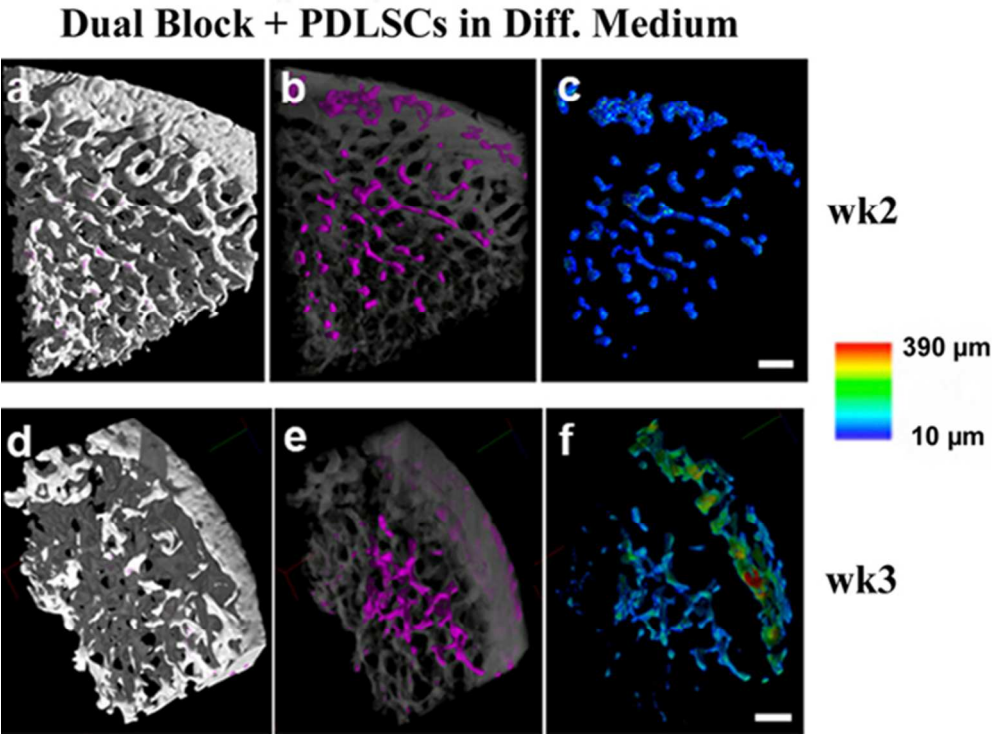
### Dual Block + PDLSCs in Basal Medium



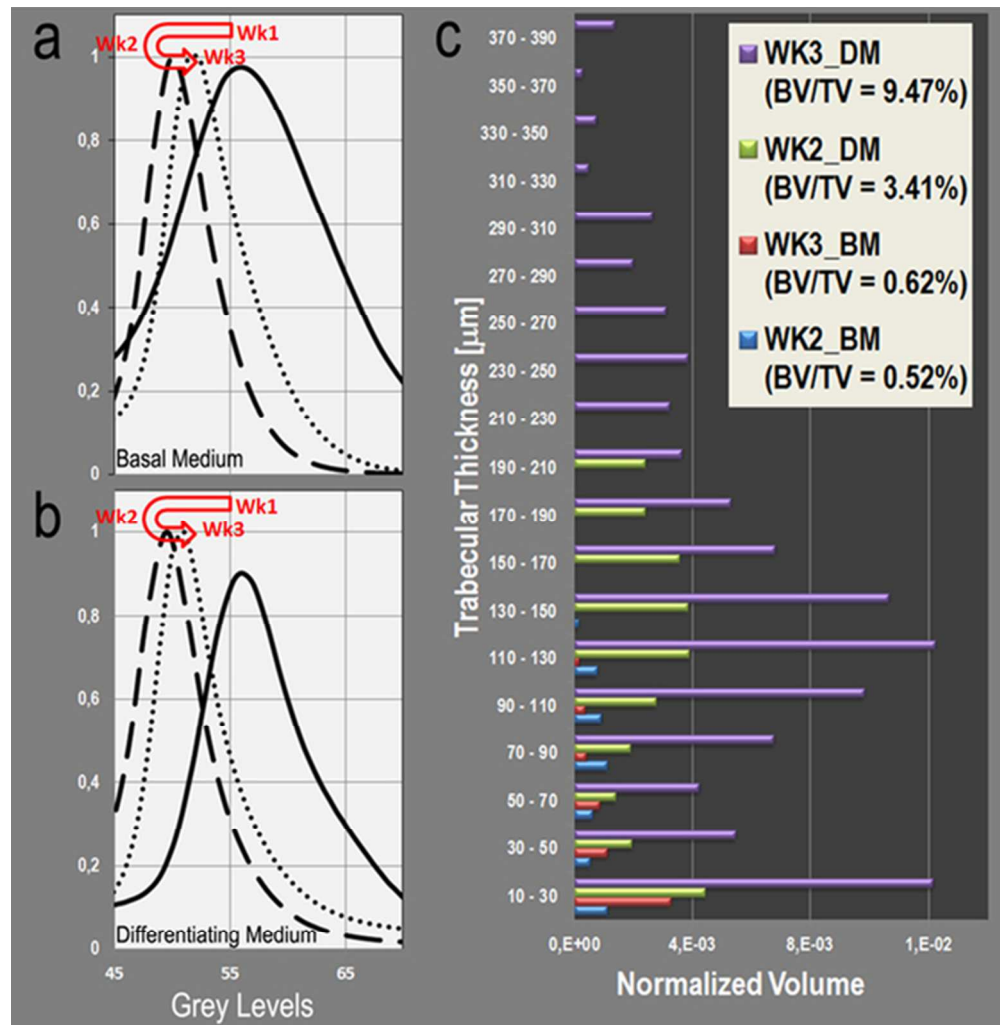
Dual block and hPDLSCs in basal medium. The interaction between cells and scaffold produces 3D Micro-CT images with two different phases, corresponding to different  $\delta$  (refractive index decrement) values. DB scaffolds are rendered in grey (panels a, b at wk2; panels d, e at wk3), whereas the contrast produced by cells - the newly-formed bone - is colored in magenta (panel b at wk2; panel e at wk3). Color map of bone thickness distribution at wk2 and wk3 are given in panel c and panel f, respectively. Thickness scale on the left. Bar: 500  $\mu\text{m}$ .

54x40mm (300 x 300 DPI)



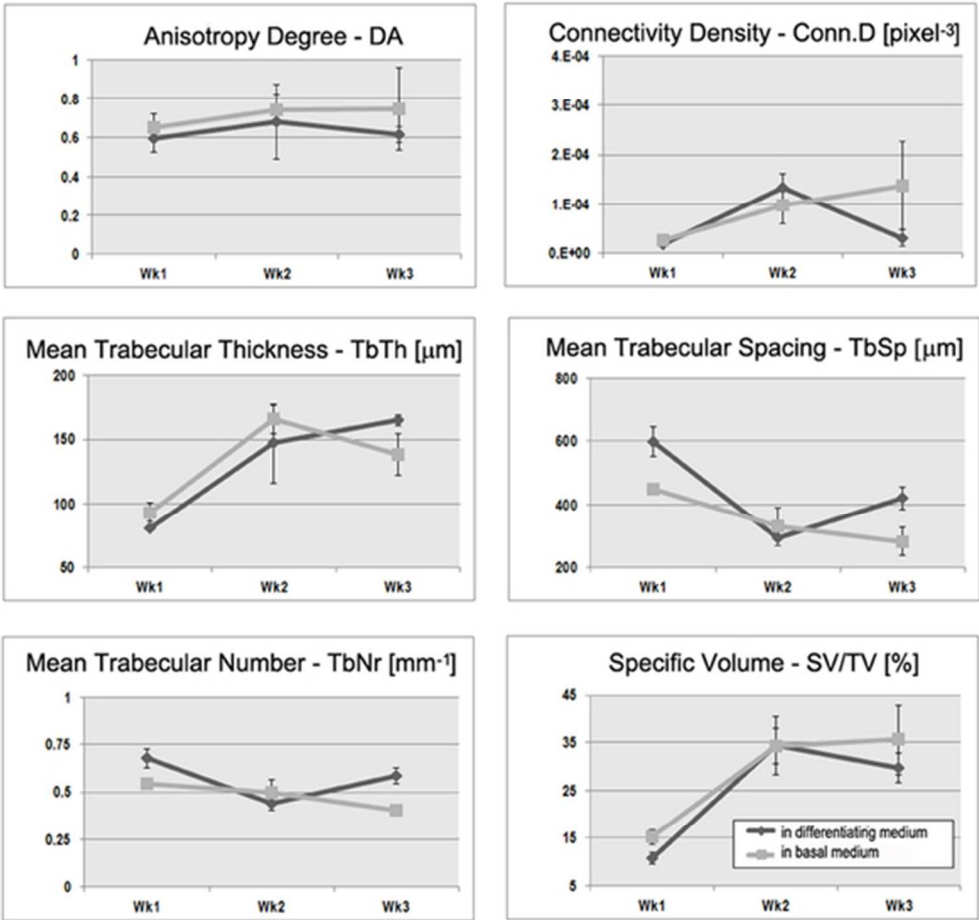


Dual block and hPDLSCs in osteogenic medium. The interaction between cells and scaffold produces 3D Micro-CT images with two different phases, corresponding to different  $\delta$  (refractive index decrement) values. DB scaffolds are rendered in grey (panels a, b at wk2; panels d, e at wk3), whereas the contrast produced by cells - the newly-formed bone - is colored in magenta (panel b at wk2; panel e at wk3). Color map of bone thickness distribution at wk2 and wk3 are given in panel c and panel f, respectively. Thickness scale on the left. Bar: 500  $\mu\text{m}$ . 54x39mm (300 x 300 DPI)



(a-b) Portion of the profile of the Intensity Counts vs. Grey Levels (proportional to the refractive index decrement  $\delta$ ). The integrated areas of the represented peaks correspond to the collagenated porcine Dual-block volume in scaffolds cultured in basal medium (panel a) and differentiating medium (panel b). In both media the contrast produced at wk2 of culture is lower than for wk1, but increases from wk2 to wk3. (c) Histograms of the distribution of the bone thickness in all the investigated samples at wk2 and wk3 of culture. The volume ratio ( $= BV/TV$ ) of the newly-formed bone structure (BV) to the total construct volume (TV) is reported in the top-right insert.

55x56mm (300 x 300 DPI)



Morphometric parameters investigated in scaffolds cultured with hPDLSCs, both in basal and differentiating media, after 1, 2 and 3 wks of culture: Anisotropy Degree (DA); Connectivity Density (Conn.D. – expressed in pixel-3); Mean Trabecular Thickness (TbTh - expressed in micrometers); Mean Trabecular Separation (TbSp - expressed in micrometers); Mean Trabecular Number (TbNr – per millimeter); Sample Volume (SV) to Total Volume (TV) ratio (SV/TV – expressed as a percentage).  
50x46mm (300 x 300 DPI)